



Proceedings of the Fifteenth International Conference on
Computational Structures Technology
Edited by: P. Iványi, J. Kruis and B.H.V. Topping
Civil-Comp Conferences, Volume 9, Paper 13.3
Civil-Comp Press, Edinburgh, United Kingdom, 2024
ISSN: 2753-3239, doi: 10.4203/ccc.9.13.3
©Civil-Comp Ltd, Edinburgh, UK, 2024

Addressing Material Softening and Strain Localization in Spatial Frame-Like Structures using Velocity-Based Beam Formulation

S. Kusuma Chandrashekhara and D. Zupan

University of Ljubljana, Slovenia

Abstract

In this paper, we propose a computational framework capable of addressing the challenges of material softening and strain localization in spatial frame-like structures. By following an alternative non-local approach and the method of embedded strong discontinuity within the original velocity-based finite element formulation, we enable the framework to identify critical load levels and critical cross-sections accurately and describe the phenomenon of strain localisation effectively. The strong discontinuity-based approach involves introducing additional jump-like variables at the level of interpolated velocities and angular velocities. These variables are governed by additional equilibrium equations at the critical cross-section, derived using the weighted residual method. Our methodology is effective for both quasi-static and dynamic analysis. The numerical examples demonstrate the effectiveness and robustness of the proposed methodologies while also showing a comparison of results between the two approaches within the same underlying beam formulation.

Keywords: strong discontinuity, material softening, post-critical analysis, strain localisation, statics and dynamics, three-dimensional rotations.

1 Introduction

In recent years, the importance of analyzing the structural response of spatial frame-like structures under severe static and dynamic loading beyond the material strength threshold has been emphasized, as material-induced localized failure is a very complex phenomenon. This failure process is often preceded by a decrease in mechanical resistance with increasing deformation, commonly referred to as softening, and is often found in brittle heterogeneous materials such as reinforced concrete. This phenomenon leads to a loss of uniqueness of cross-sectional constitutive equations and loss of ellipticity/hyperbolicity of equilibrium equations. One important consequence of strain softening is the localization of strains and rapid jumps in the displacement field. If not appropriately modeled, the numerical solution procedure often leads to a loss of convergence at the critical load level and mesh-dependent post-peak responses.

In the present work, we demonstrate the phenomenon of softening and localization of strains within spatial frame-like structures using two different approaches. In the first approach, we use an alternative non-local method where the strains are assumed to be concentrated within the entire finite element of short length rather than at a point. This approach is simple and effective, capable of simulating the softening response while resolving strain localization at critical cross-sections using short, lower-order elements. The second approach follows the idea of embedded discontinuity, where the primary interpolated variables are enhanced to describe localized strains as point-wise peak-like distributions.

These methodologies are implemented within geometrically exact spatial beam finite elements, where the tangent space of the non-linear configuration space is spanned using only additive quantities, which are velocities in the fixed basis and angular velocities in the local basis. We demonstrate the efficiency of both approaches through a demanding numerical example with a detailed comparison.

2 Mathematical model

The geometry of a three-dimensional beam is represented by a line of centroids and a family of cross sections, see Figure 1. The line of centroids is a spatial curve at an arbitrary time $t \geq 0$ defined by a position vector $\vec{r}(x, t)$ and parametrized by an arc-length parameter $x \in [0, L]$ at any fixed time t . Two orthogonal reference frames are introduced for the description of the quantities of the beam: (i) a fixed orthogonal basis represented by $\{\vec{g}_1, \vec{g}_2, \vec{g}_3\}$ at the reference point \mathcal{O} and (ii) local orthogonal base vectors $\{\vec{G}_1, \vec{G}_2, \vec{G}_3\}$. A transformation from the local basis to the fixed one is described in terms of quaternion algebra as:

$$\vec{G}_i(x, t) = \hat{q}(x, t) \circ \vec{g}_i \circ \hat{q}^*(x, t), \quad (1)$$

where \hat{q} is a rotational quaternion, \hat{q}^* is its conjugate, and (\circ) denotes the quaternion product.

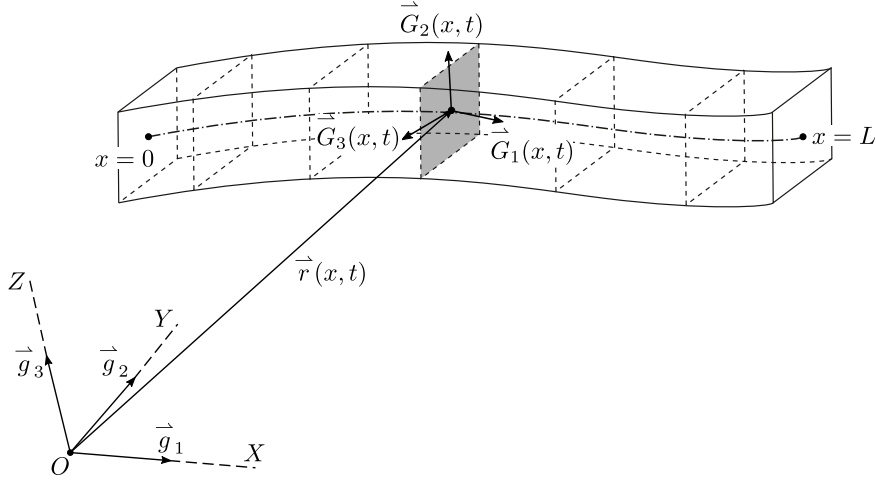


Figure 1: Configuration of a three dimensional beam at an arbitrary time t .

The equations of a quaternion-based three dimensional beam within the framework of velocity-based formulation together with the discretization procedure are presented in [1] while for the formulation consistent post-critical analysis using path-following approach, the reader is addressed to [2] and the discussion therein. In the present paper, we focus on the phenomenon of strain softening and modelling the localisation of strains.

2.1 Equations of a three-dimensional beam

In this section, we briefly outline the governing equations of a three-dimensional beam in terms of quaternion algebra. For more details, the reader is directed to [1]. The set of continuous governing equations for a three-dimensional beam consists of kinematic equations (2)-(7), constitutive equations (8)-(9), and equilibrium equations (10)-(11):

$$\mathbf{\Gamma} = \hat{\mathbf{q}}^* \circ \mathbf{r}' \circ \hat{\mathbf{q}} + \mathbf{\Gamma}_0, \quad (2)$$

$$\mathbf{K} = 2\hat{\mathbf{q}}^* \circ \hat{\mathbf{q}}' + \mathbf{K}_0, \quad (3)$$

$$\mathbf{v} = \dot{\mathbf{r}}, \quad (4)$$

$$\mathbf{\Omega} = 2\hat{\mathbf{q}}^* \circ \dot{\hat{\mathbf{q}}}, \quad (5)$$

$$\dot{\mathbf{\Gamma}} = \hat{\mathbf{q}}^* \circ \mathbf{v}' \circ \hat{\mathbf{q}} + (\mathbf{\Gamma} - \mathbf{\Gamma}_0) \times \mathbf{\Omega}, \quad (6)$$

$$\dot{\mathbf{K}} = \mathbf{\Omega}' + \mathbf{K} \times \mathbf{\Omega}. \quad (7)$$

$$\mathbf{N} = \mathcal{C}_{\mathcal{N}}(\mathbf{\Gamma}, \mathbf{K}), \quad (8)$$

$$\mathbf{M} = \mathcal{C}_{\mathcal{M}}(\mathbf{\Gamma}, \mathbf{K}), \quad (9)$$

$$\mathbf{n}' + \tilde{\mathbf{n}} = \rho A \dot{\mathbf{v}}, \quad (10)$$

$$\mathbf{M}' + \mathbf{K} \times \mathbf{M} + (\mathbf{\Gamma} - \mathbf{\Gamma}_0) \times \mathbf{N} + \hat{\mathbf{q}}^* \circ \tilde{\mathbf{m}} \circ \hat{\mathbf{q}} = \mathbf{\Omega} \times \mathbf{J}_\rho \mathbf{\Omega} + \mathbf{J}_\rho \dot{\mathbf{\Omega}}, \quad (11)$$

where the prime (\prime) denotes the derivative with respect to the arc-length parameter x and the dot over symbol ($\dot{\cdot}$) denotes the derivative with respect to time t . The vector

quantities expressed in fixed basis are denoted with lower case letters while the ones in the local basis are denoted with upper case letters. In the above equations,

\mathbf{I} represents the vector of translational strains (I_1 is the extensional strain, I_2 and I_3 are the shear strains);

\mathbf{K} represents the vector of rotational strains (K_1 is the torsional strain, K_2 and K_3 are the bending strains);

\mathbf{r} and $\hat{\mathbf{q}}$ represent position vector and rotational quaternion, respectively;

\mathbf{I}_0 and \mathbf{K}_0 are the variational constants derived from the known position vectors, strains and rotations at the initial configuration;

\mathbf{v} is the velocity vector and $\mathbf{\Omega}$ is the vector of angular velocity;

\mathbf{N} and \mathbf{M} are the vectors of stress-resultant forces and moments of the cross-section;

\mathcal{C}_N and \mathcal{C}_M are operators describing the material of the beam;

$\tilde{\mathbf{n}}$ and $\tilde{\mathbf{m}}$ are the vectors of external distributed forces and moments per unit length of the undeformed beam;

ρ and \mathbf{J}_ρ represent mass density and mass moment of inertia of the cross-section, respectively.

Equations (6)-(7) represent kinematic compatibility equations which directly relate strains with velocities and angular velocities and therefore play an important role in the present velocity-based approach [3]. Equations (10)-(11) are the linear and angular momentum balance equations. Note that the balance of linear momentum of a beam is expressed in fixed basis while the balance of angular momentum is expressed in local basis. Consequently, the following boundary conditions that need to be satisfied by the set of governing equations are also expressed according to the present choice of bases:

$$\mathbf{n}(0) + \mathbf{f}_e^0 = \mathbf{0}, \quad (12)$$

$$\mathbf{n}(L) - \mathbf{f}_e^L = \mathbf{0}, \quad (13)$$

$$\mathbf{M}(0) + \hat{\mathbf{q}}^*(0) \circ \mathbf{m}_e^0 \circ \hat{\mathbf{q}}(0) = \mathbf{0}, \quad (14)$$

$$\mathbf{M}(L) - \hat{\mathbf{q}}^*(L) \circ \mathbf{m}_e^L \circ \hat{\mathbf{q}}(L) = \mathbf{0}, \quad (15)$$

where \mathbf{f}_e^0 , \mathbf{m}_e^0 , \mathbf{f}_e^L and \mathbf{m}_e^L are known external point forces and moments at the boundaries of the beam element.

2.2 Material nonlinearity

In the beam models stresses are replaced by stress-resultants and the constitutive equations are represented at the resultant level as shown in the equations (8)-(9). However, well established experimental techniques characterize material behaviour at the continuum-based stress-strain level. In order to incorporate such constitutive behavior we span the resultant strain measures over the cross-section according to the relation:

$$D(y, z) = \Gamma_1 - yK_3 + zK_2, \quad (16)$$

where D is the longitudinal strain, y and z are the local coordinates of the cross-section defined by the base vectors \vec{G}_2 and \vec{G}_3 (see Figure 1). The longitudinal stress, $\sigma(y, z)$ at an arbitrary material fiber of the cross-section, can now be assumed to be a function of the strain field:

$$\sigma(y, z) = \mathcal{F}(D(y, z)). \quad (17)$$

The functional \mathcal{F} in the above equation can be estimated from the uni-axial experiments while many are already recommended in literature and engineering codes. However, when examining the structural response using material models that incorporate a plastic regime, it becomes crucial to differentiate between elastic and plastic deformations. This distinction is necessary to accurately account for irreversible plastic strain during unloading. The Kuhn-Tucker unilateral constraint offers a convenient formulation for loading and unloading in classical rate-independent plasticity. The incremental form and the algorithmic implementation of the loading/unloading conditions as presented in [4] was here properly extended to material models used. To evaluate the resultant quantities, the stress field needs to be integrated over the cross-sectional plane (y, z) while for shear and torsion, we assume linear relationship:

$$\mathbf{C}_{\mathcal{N}} = \begin{bmatrix} N_1^C \\ N_2^C \\ N_3^C \end{bmatrix} = \begin{bmatrix} \iint \sigma(D) dy dz \\ GA_2 \Gamma_2 \\ GA_3 \Gamma_3 \end{bmatrix}, \quad (18)$$

$$\mathbf{C}_{\mathcal{M}} = \begin{bmatrix} M_1^C \\ M_2^C \\ M_3^C \end{bmatrix} = \begin{bmatrix} GJ_t K_1 \\ \iint z \sigma(D) dy dz \\ - \iint y \sigma(D) dy dz \end{bmatrix}, \quad (19)$$

where G is the shear modulus, A_2 and A_3 are effective shear areas and J_t is the torsional moment of inertia. Taking the partial derivatives of equations (18)-(19) with respect to the components of resultant strain measures, we get the constitutive tangent matrix that reads:

$$\mathbb{C} = \begin{bmatrix} \mathbb{C}_{\Gamma\Gamma} & \mathbb{C}_{\Gamma K} \\ \mathbb{C}_{K\Gamma} & \mathbb{C}_{KK} \end{bmatrix} = \begin{bmatrix} \frac{\partial \mathbf{C}_{\mathcal{N}}}{\partial \Gamma} & \frac{\partial \mathbf{C}_{\mathcal{N}}}{\partial \mathbf{K}} \\ \frac{\partial \mathbf{C}_{\mathcal{M}}}{\partial \Gamma} & \frac{\partial \mathbf{C}_{\mathcal{M}}}{\partial \mathbf{K}} \end{bmatrix}. \quad (20)$$

The unique solution of equations (8) and (9) exists when the determinant of the Jacobian matrix is not singular. As the deformation increases, the Jacobian matrix, \mathbb{C} ,

approaches zero value at a specific cross-section, denoted by the coordinate x_c . Upon further deformation at this critical cross-section, the determinant of matrix \mathbb{C} in the post-critical stage turns negative, which is a typical characteristic of the softening regime.

2.3 Numerical formulation

The governing equations of a three-dimensional beam are a set of nonlinear partial differential equations that needs to be discretized in both time and space. The configuration space of the primary unknowns is crucial in any finite element formulation. While standard configuration-based formulations (displacement and rotation-based models) are convenient, their use has several limitations. For instance, the additive-type interpolation for rotational parameters is simple but fundamentally contradicts the configuration space of spatial rotations, which is multiplicative.

To avoid the need for special adaptations of integration schemes or interpolation procedures for the rotational degrees of freedom, we leverage the additive nature of the angular velocities when expressed in the local basis. This allows us to employ standard additive-type enhancements and standard interpolation in Euclidean vector spaces directly. This choice significantly reduces computational complexity and avoids introducing any inconsistencies. For the translational degrees of freedom, using velocities in the fixed basis is a natural choice. Finally the chosen approximations of both translational and rotational parameters that are consistent with the properties of the configuration space read:

$$\mathbf{v}(x, t) = \sum_{i=1}^p P_i(x) \mathbf{v}_i(t), \quad (21a)$$

$$\boldsymbol{\Omega}(x, t) = \sum_{i=1}^p P_i(x) \boldsymbol{\Omega}_i(t). \quad (21b)$$

We here choose Lagrange interpolation functions with the nodes taken equidistantly from the interval $[0, L]$.

2.4 Enhanced interpolation

At the onset of localization at the critical cross-section x_c , the above velocity and angular velocity fields (21a)-(21b) are enriched with a unit step function at the critical cross-section x_c multiplied by velocity and angular velocity jumps $\Delta \mathbf{v}$ and $\Delta \boldsymbol{\Omega}$:

$$\mathbf{v}(x, t) = \sum_{i=1}^p P_i(x) \mathbf{v}_i(t) + \left(H(x - x_c) - \sum_j P_j(x) \right) \Delta \mathbf{v}(t), \quad (22a)$$

$$\boldsymbol{\Omega}(x, t) = \sum_{i=1}^p P_i(x) \boldsymbol{\Omega}_i(t) + \left(H(x - x_c) - \sum_j P_j(x) \right) \Delta \boldsymbol{\Omega}(t). \quad (22b)$$

Here, $H(x - x_c)$ is the Heaviside step function defined as:

$$H_c = H(x - x_c) = \begin{cases} 0, & x < x_c, \\ 1, & x \geq x_c. \end{cases}$$

It can be observed from (6)-(7) that the description of translational and rotational strains directly involves the derivatives of velocities and angular velocities at midtime. They can be directly expressed by differentiating the assumed velocity and angular velocity in equations (22a)-(22b):

$$\mathbf{v}'(x) = \sum_{i=1}^p P_i'(x) \mathbf{v}_i + \left(\delta_c(x) - \sum_j P_j'(x) \right) \Delta \mathbf{v}, \quad (23a)$$

$$\mathbf{\Omega}'(x) = \sum_{i=1}^p P_i'(x) \mathbf{\Omega}_i + \left(\delta_c(x) - \sum_j P_j'(x) \right) \Delta \mathbf{\Omega}, \quad (23b)$$

where, $\delta_c(x)$ is the Dirac delta function (distribution) and will here serve as a generalized function that allows us to overcome problems with singularities of the derivatives at the critical point. The time discretization is according to midpoint rule and the spatial discretization follows Galerkin finite element method. For the sake of brevity, we present here the final discretized equations of motion however, for a comprehensive understanding, the reader is addressed to [1]. The final discretized governing equations read:

$$\int_0^L \left[\frac{\rho A}{h} (\mathbf{v}^{[n+1]} - \mathbf{v}^{[n]}) P_i + P_i' \mathbf{n}^{[n+1/2]} - P_i \tilde{\mathbf{n}}^{[n+1/2]} \right] dx - \mathbf{e} \mathbf{f}_i^{[n+1/2]} = \mathbf{0}, \quad (24)$$

$$\begin{aligned} & \int_0^L \left[\frac{\mathbf{J}_\rho}{h} (\mathbf{\Omega}^{[n+1]} - \mathbf{\Omega}^{[n]}) P_i + \mathbf{M}^{[n+1/2]} P_i' - \mathbf{K}^{[n+1/2]} \times \mathbf{M}^{[n+1/2]} P_i \right. \\ & + \mathbf{\Omega}^{[n+1/2]} \times \mathbf{J}_\rho \mathbf{\Omega}^{[n+1/2]} P_i - \left(\mathbf{\Gamma}^{[n+1/2]} - \mathbf{\Gamma}_0 \right) \times \mathbf{N}^{[n+1/2]} P_i \\ & \left. - \left(\hat{\mathbf{q}}^{*[n+1/2]} \circ \tilde{\mathbf{m}}^{[n+1/2]} \circ \hat{\mathbf{q}}^{[n+1/2]} \right) P_i \right] dx - \mathbf{e} \mathbf{M}_i^{[n+1/2]} = \mathbf{0}, \end{aligned} \quad (25)$$

$$\begin{aligned} & \int_{x_c}^L \left[\frac{\rho A}{h} (\mathbf{v}^{[n+1]} - \mathbf{v}^{[n]}) - \tilde{\mathbf{n}}^{[n+1/2]} \right] dx + \mathbf{n}(x_c)^{[n+1/2]} - \mathbf{n}(L)^{[n+1/2]} \\ & - \int_0^L \left[\left(\frac{\rho A}{h} (\mathbf{v}^{[n+1]} - \mathbf{v}^{[n]}) - \tilde{\mathbf{n}}^{[n+1/2]} \right) \sum_j P_j + \sum_j P_j' \mathbf{n}^{[n+1/2]} \right] dx \\ & + \sum_j P_j(L) \mathbf{n}(L)^{[n+1/2]} - \sum_j P_j(0) \mathbf{n}(0)^{[n+1/2]} = \mathbf{0}, \end{aligned} \quad (26)$$

$$\begin{aligned}
& \int_{x_c}^L \left[\frac{\mathbf{J}_\rho}{h} \left(\boldsymbol{\Omega}^{[n+1]} - \boldsymbol{\Omega}^{[n]} \right) + \boldsymbol{\Omega}^{[n+1/2]} \times \mathbf{J}_\rho \boldsymbol{\Omega}^{[n+1/2]} - \mathbf{K}^{[n+1/2]} \times \mathbf{M}^{[n+1/2]} \right. \\
& \left. - \left(\boldsymbol{\Gamma}^{[n+1/2]} - \boldsymbol{\Gamma}_\theta \right) \times \mathbf{N}^{[n+1/2]} - \hat{\mathbf{q}}^{*[n+1/2]} \circ \tilde{\mathbf{m}}^{[n+1/2]} \circ \hat{\mathbf{q}}^{[n+1/2]} \right] dx \\
& - \left\{ \int_0^L \left[\frac{\mathbf{J}_\rho}{h} \left(\boldsymbol{\Omega}^{[n+1]} - \boldsymbol{\Omega}^{[n]} \right) \sum_j P_j - \left(\boldsymbol{\Gamma}^{[n+1/2]} - \boldsymbol{\Gamma}_\theta \right) \times \mathbf{N}^{[n+1/2]} \sum_j P_j \right. \right. \\
& \left. \left. - \hat{\mathbf{q}}^{*[n+1/2]} \circ \tilde{\mathbf{m}}^{[n+1/2]} \circ \hat{\mathbf{q}}^{[n+1/2]} \sum_j P_j + \boldsymbol{\Omega}^{[n+1/2]} \times \mathbf{J}_\rho \boldsymbol{\Omega}^{[n+1/2]} \sum_j P_j \right. \right. \\
& \left. \left. - \mathbf{K}^{[n+1/2]} \times \mathbf{M}^{[n+1/2]} \sum_j P_j + \mathbf{M}^{[n+1/2]} \sum_j P'_j \right] dx \right\} + \mathbf{M}(x_c)^{[n+1/2]} \\
& - \mathbf{M}(L)^{[n+1/2]} + \sum_j P_j(L) \mathbf{M}(L)^{[n+1/2]} - \sum_j P_j(0) \mathbf{M}(0)^{[n+1/2]} = \mathbf{0}.
\end{aligned} \tag{27}$$

where $e\mathbf{f}_i^{[n+1/2]}$ and $e\mathbf{M}_i^{[n+1/2]}$ are evaluated as:

$$e\mathbf{f}_i^{[n+1/2]} = \begin{cases} \mathbf{f}_e^0(t_{n+1/2}), & i = 1 \\ \mathbf{f}_e^L(t_{n+1/2}), & i = p \\ \mathbf{0}, & \text{otherwise} \end{cases}$$

$$e\mathbf{M}_i^{[n+1/2]} = \begin{cases} \hat{\mathbf{q}}^{*[n+1/2]} \circ \mathbf{m}_e^0(t_{n+1/2}) \circ \hat{\mathbf{q}}^{[n+1/2]}, & i = 1 \\ \hat{\mathbf{q}}^{*[n+1/2]} \circ \mathbf{m}_e^L(t_{n+1/2}) \circ \hat{\mathbf{q}}^{[n+1/2]}, & i = p \\ \mathbf{0}, & \text{otherwise.} \end{cases}$$

Since the set of discrete equations (24)-(27) is nonlinear, they are solved iteratively using the Newton-Raphson method. The linearization required due to the presence of rotational degrees of freedom is straightforward and has therefore been omitted here. One of the crucial aspect within the method of embedded discontinuities is to suitably approximate the Dirac-delta distribution that appears in the equations (23a)-(23b). The assumption here follows,

$$\delta_c(x_i) = \delta(x_i - x_c) = \begin{cases} \frac{1}{h_c}, & x_i = x_c, \\ 0, & \text{otherwise,} \end{cases} \tag{28}$$

where h_c is a material parameter.

3 Numerical example: Cranston's frame

In this example, a hinged planar reinforced concrete frame is subjected to symmetric loading. The frame's geometric and cross-sectional data can be found in Figure 2.

This particular frame was experimentally tested by Cranston [5], and serves here for validation.

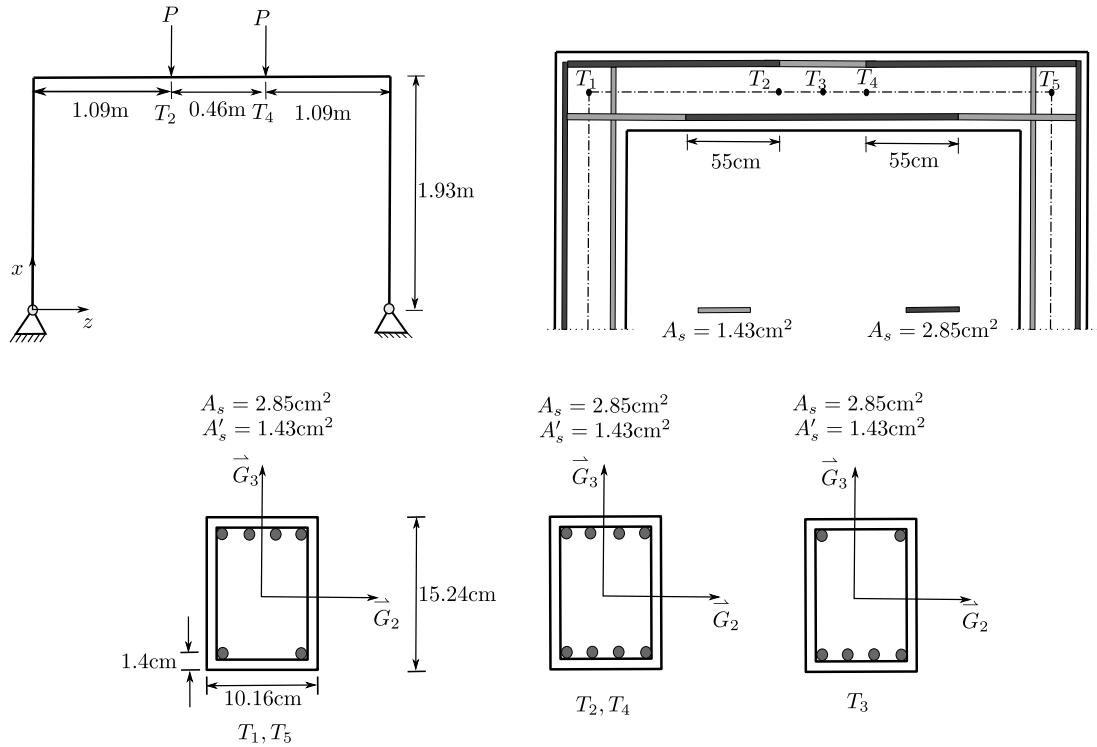


Figure 2: Cranston's portal frame: geometry.

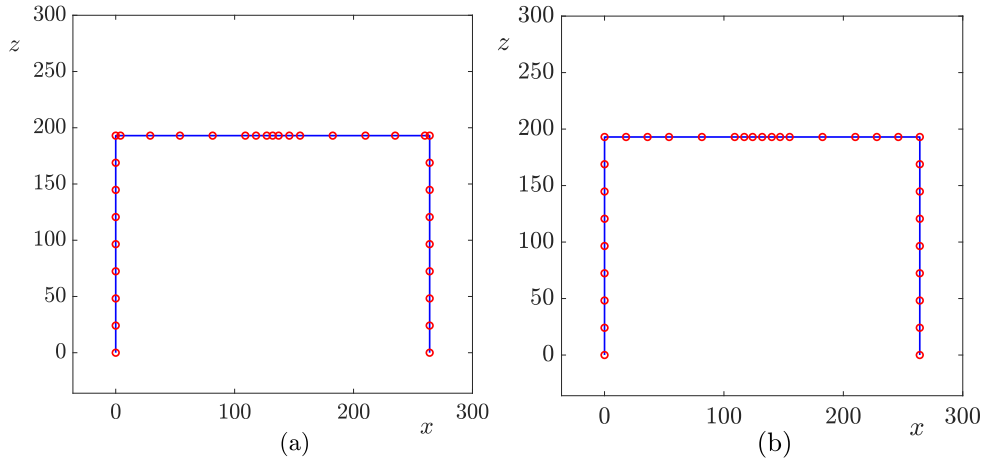


Figure 3: Cranston's portal frame: Mesh for non-local and embedded discontinuity approach (nodes are marked with red circles).

The constitutive relationship for concrete here follows the model of Desayi and Krishnan [7] with additional considerations for tensile behavior as provided by Bergan

and Holland [6]. The analytical relation reads:

$$\sigma(D) = \begin{cases} 0, & D \leq D_{cu} \\ 2f_{cm}|D_1|\frac{D}{D^2+D_1^2}, & D_{cu} < D \leq D_r \\ \frac{f_{ct}}{D_r-D_m}(D-D_m), & D_r < D \leq D_m \\ 0, & D_m < D. \end{cases} \quad (29)$$

The behavior of reinforcing steel in tension and compression is described as:

$$\sigma_s(D) = \begin{cases} E_s D, & |D| \leq D_{y1} \\ (f_y + E_p(|D| - D_{y1}))\text{sign}(D), & D_{y1} < |D| \leq D_{y2} \\ (f_y + E_p(D_{y2} - D_{y1}))\text{sign}(D) \left(1 - \frac{|D|-D_{y2}}{D_{yu}-D_{y2}}\right), & D_{y2} < |D| \leq D_{yu} \\ 0, & |D| > D_{yu}. \end{cases} \quad (30)$$

The material parameters used in the present analysis are: $f_{cm} = 3.65 \text{ kN/cm}^2$, $f_y = 29.3 \text{ kN/cm}^2$, $E_{cm} = 3180 \text{ kN/cm}^2$, $E_s = 18000 \text{ kN/cm}^2$, $E_p = 200 \text{ kN/cm}^2$, $G = 1312.5 \text{ kN/cm}^2$, $D_{cu} = -0.05$, $D_1 = -0.0022$, $D_r = 5.5 \times 10^{-5}$, $D_m = 7 \times 10^{-4}$, $D_{y2} = 0.01$, $D_{yu} = 1.0$. The tensile strength (f_{ct}) in equation (29) is calculated using the following relation: $f_{ct} = (2f_{cm}|D_r|)D / (D_r^2 + D_1^2)$. The results obtained using both non-local and embedded discontinuities approaches are presented here. For the non-local approach, a mesh of 32 quadratic elements was used, while cubic elements were used for the method of embedded discontinuities. To account for the sudden change in the number of reinforcement bars between T_1 and T_5 , shorter elements were used to model the horizontal section. The mesh for both methods is illustrated in Figure 3. Cross-sectional integrals were evaluated using 100×100 Gaussian points. The width of the localization zone was set to $h_c = 4 \text{ cm}$, and for the non-local approach, short elements of the same length were employed near potential critical cross-sections, as shown in Figure 3. One of the important issue in analysing the structural response at the onset of material softening is to overcome the global singularity. Path-following constraint described in [2] can be directly employed within the present formulation to overcome this issue. However, in the present analysis, the mass matrix is conveniently considered and thus circumvents the singularity of the global system and eliminates the need for any additional constraint.

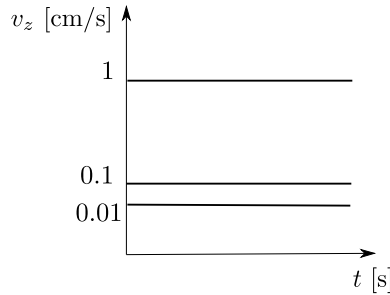


Figure 4: Prescribed velocities at T_2 and T_4 (see Figure 4).

The frame is subjected to vertical forces as shown in Figure 2. However, the present dynamic formulation allows to enforce velocities at the position of applied forces (T_2 and T_4) and follow a dynamic response of the frame as an alternative. The material density is taken to be $\rho = 2200 \text{ kg/m}^3$. The vertical displacements are enforced with three different rates: (i) 0.01 cm/s, (ii) 0.1 cm/s, (iii) 1 cm/s. For the present results constant velocities were prescribed at T_2 and T_4 (see Figure 4) resulting in linear displacements at the same nodes. The results were calculated until a vertical displacement of 6 cm was reached at the mid span T_3 . The load factor is here estimated from the differences of shear forces at the nodes where the velocities are enforced. In the present analysis, softening initiates at the cross-sections T_1 , T_2 and T_5 . The obtained load-displacement responses are shown in the Figure 5(a) and are compared to the experimental results as well as the result obtained using the path-constraint (black solid line). We can observe that the pre-critical response is similar for all three cases. As expected, the slower velocity results are closer to the quasi-static response, while the post-critical response shows a significant reduction in load-bearing capacity and slower initiation of horizontal displacements with increasing velocity (see Figure 5(b)).

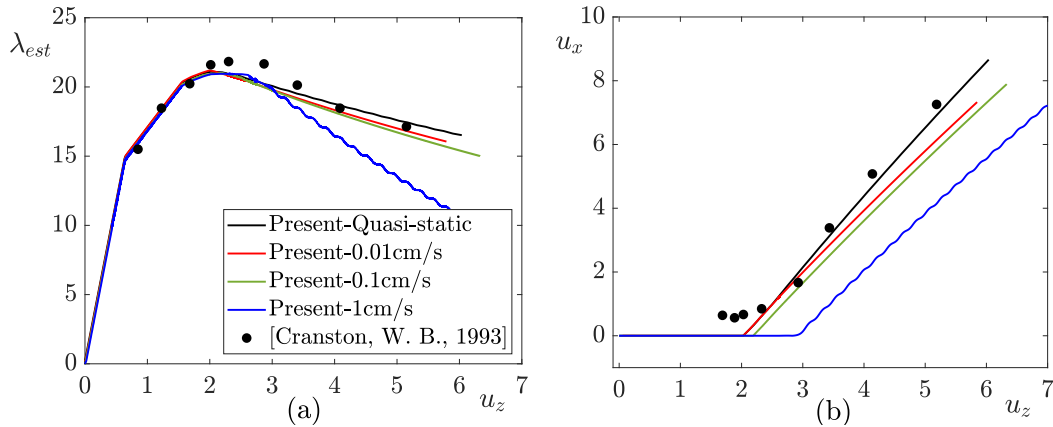
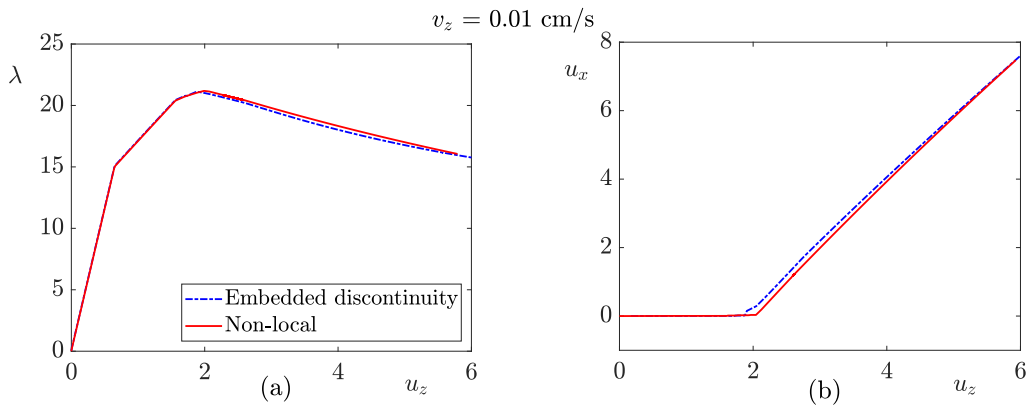


Figure 5: Influence of displacement rate: (a) Load factor vs. vertical displacements at T_3 ; (b) horizontal vs. vertical displacements at T_3 .



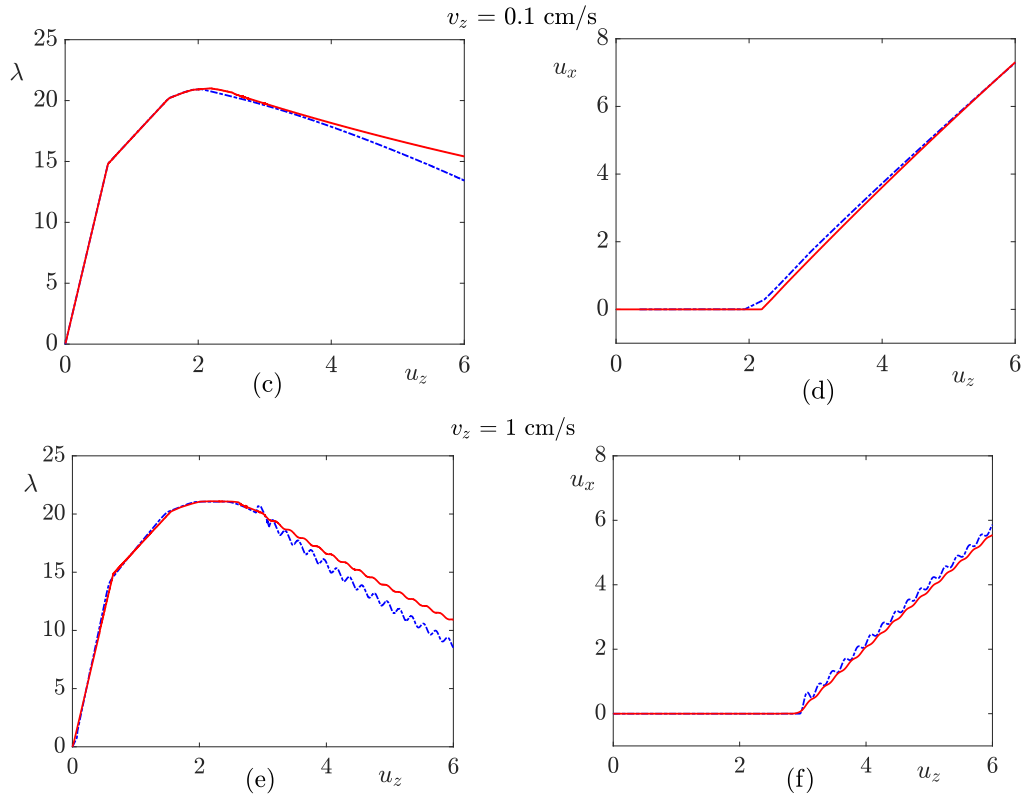
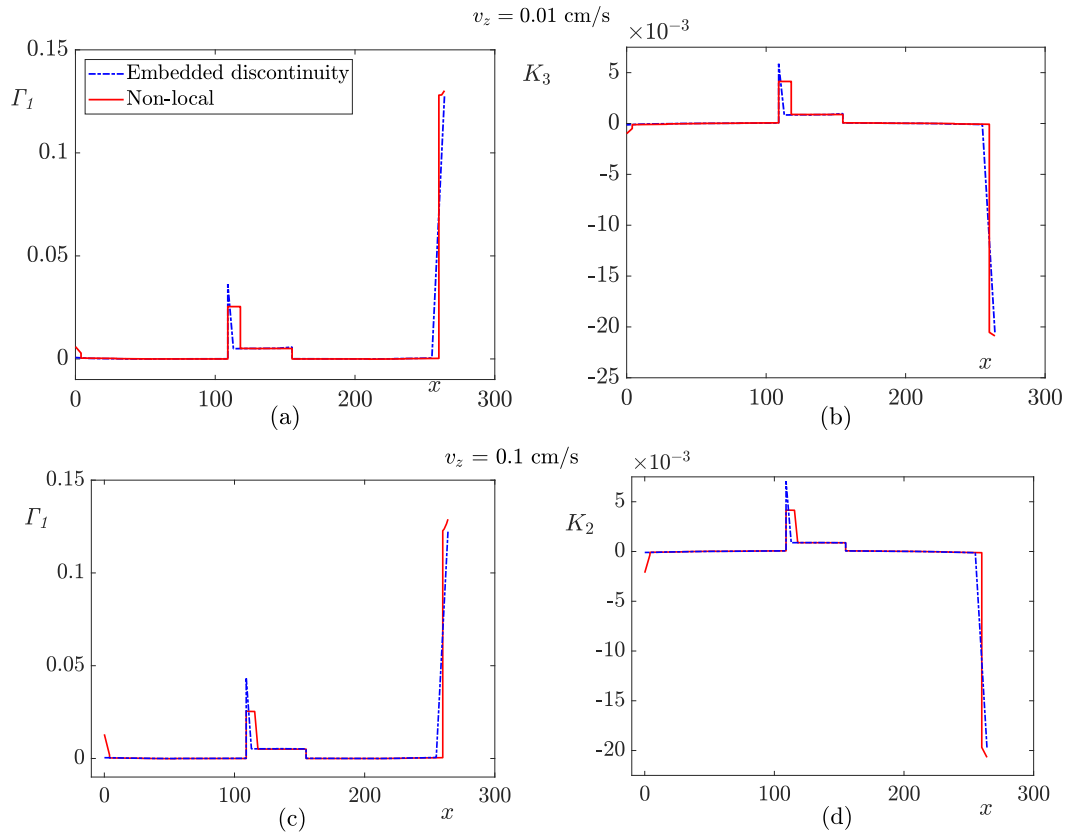


Figure 6: Comparison between non-local and embedded discontinuity approach: (a,c,e) Load factor vs. vertical displacements at T_3 ; (b,d,f) horizontal vs. vertical displacements at T_3 .



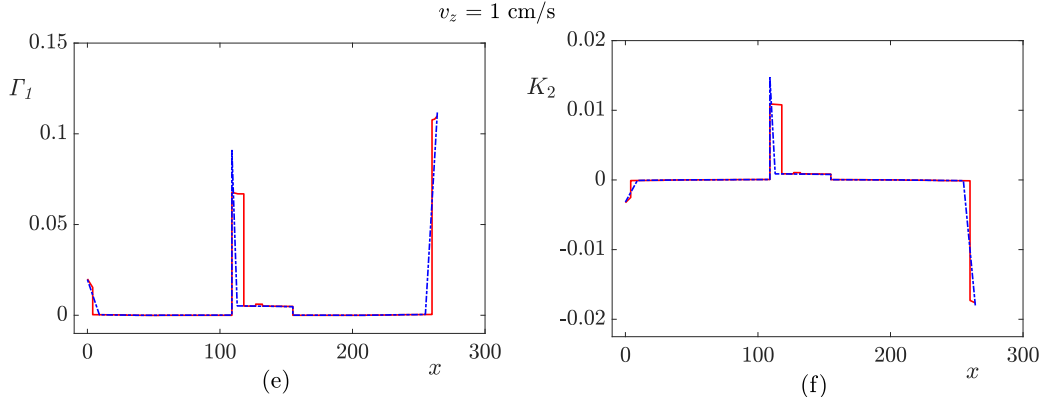


Figure 7: Comparison of longitudinal and bending strain distributions between non-local and embedded discontinuity approach at 6 cm deflection of mid-span T_3 .


Furthermore, the comparison of results between the method of embedded discontinuities and the non-local approach are shown in the Figures 6 and 7. It can be observed from the load-displacement response (see Figure 6) that there is a significant difference in the post-critical regime for higher velocity between the two approaches. This can be explained through the longitudinal and bending strain distribution along the horizontal beam. The non-local approach under predicts the strains at the softened cross-section T_2 when compared to the method embedded discontinuities. It is additionally interesting to observe that at higher velocity, the longitudinal and bending strains at the cross-section T_2 become significantly large when compared to the lower velocities. Both approaches are able to describe the localisation of strains effectively. While the non-local approach distribute the longitudinal and bending strains over the entire element, the method of embedded discontinuities clearly describe the point-wise localisation of strains at the softened cross-sections.

4 Conclusion

In the present work, the original velocity-based formulation is extended for the analysis of material softening, introducing several conceptually unique characteristics. The formulation employs velocities in a fixed basis and angular velocities in a local basis as the only interpolated quantities along the length of a beam element. The introduced additive-type enhancements are fully consistent with the properties of the configuration space. In the non-local approach, strain localization is achieved by using short, low-order elements, with strains concentrated within a finite but short length in the neighborhood of critical cross-sections rather than at a point, meaning the localization of strains solely depends on the length parameter. Meanwhile, the method of embedded discontinuities describes the localization of strains as a point-wise peak-like distribution, circumventing dependency on the mesh. Additionally, the mass matrix directly enables overcoming the global singularity at the onset of material softening

without the need for any additional constraints. The demonstrated numerical example shows the effectiveness and robustness of the proposed approaches.

Acknowledgements

This work was supported by the European Union’s Horizon 2020 research and innovation programme under the Marie Skłodowska-Curie grant agreement No. 860124. This publication reflects only the author’s view and the Research Executive Agency is not responsible for any use that may be made of the information it contains. 

References

- [1] E. Zupan, D. Zupan, “On conservation of energy and kinematic compatibility in dynamics of nonlinear velocity-based three-dimensional beams”, *Nonlinear Dynamics*, 95, 1379-1394, 2019.
- [2] S. Kusuma Chandrashekhara, D. Zupan, “Path following using velocity-based approach in quasi-static analysis”, *International Journal of Solids and Structures*, 275, 112292, 2023.
- [3] S.S. Antman, “Invariant dissipative mechanisms for the spatial motion of rods suggested by artificial viscosity”, *Journal of Elasticity*, 70, 55-64, 2003.
- [4] J.C. Simo, T.J.R. Hughes, *Computational Inelasticity*, Springer, New York, 1998.
- [5] W.B. Cranston, A computer method for inelastic analysis of plane frames, 386, *Cement and Concrete Association*, 1965.
- [6] P.G. Bergan, I. Holland, “Nonlinear finite element analysis of concrete structures”, *Computer Methods in Applied Mechanics and Engineering*, 17/18, 443-467, 1979.
- [7] P. Desayi, S. Krishnan, “Equation for the Stress-Strain Curve of Concrete”, *ACI Journal Proceedings*, 61, 345-350, 1964.